Supplementary Materials for

C–N Bond Formation from Co-Conversion of N_2 and CO_2 Mediated by $Nb_2OH_4^-$ Cluster Anions: Importance of Hydride Ligands

Xiao-Xiao Liu,[1,2,3] Qing-Yu Liu,[1,3] Zi-Yu Li,[1,3,] Sheng-Gui He[1,2,3]*

[1] State Key Laboratory for Structural Chemistry of Unstable and Stable Species, Institute of Chemistry, Chinese Academy of Sciences, Beijing, 100190, P. R. China

[2] University of Chinese Academy of Sciences, Beijing, 100049, P. R. China

[3] Beijing National Laboratory for Molecular Sciences and CAS Research/Education Centre of Excellence in Molecular Sciences, Beijing, 100190, P. R. China

Table of Contents

1. Methods

1.1 Experimental Details

Mass spectrometry. A schematic diagram of the experimental apparatus used in this study is shown in Figure S1. The niobium hydride clusters ($Nb_xO_yH_z^-$) were generated by laser ablation of a niobium foil with the surface slightly oxidized in the presence of 1% H_2 seeded in a He carrier gas with the backing pressure of 6 standard atmospheres. A 532 nm (second harmonic Nd^{3+}:YAG) laser with energy of 15−20 mJ/pulse and repetition rate of 10 Hz was used. A newly developed double ion trap system, including two quadrupole mass filters (QMFs) and two linear ion trap (LIT) reactors that enable the injection of different reactants spatially separated, was employed to investigate the sequential reactions of cluster ions with dinitrogen and carbon dioxide.[1] The clusters of interest $Nb_2OH_4^-$ were mass-selected by QMF1 and then entered LIT1, where they were confined and cooled by collisions with a pulse of buffer gas (He) and then interacted with another pulse of N_2. After the $Nb_2OH_4^-$ ions reacting with N_2, the resulting $Nb_2OH_2N_2^-$ and $Nb_2ON_2^-$ product ions were mass selected by the QMF2 and then injected into LIT2 for reacting with diluted CO_2. The temperature of the cooling gas (He), reactant gases (N_2 and CO_2), and the LIT reactors was around 298 K. After the reaction took place in the reactor, the reactant and product ions were ejected from the trap and entered into a reflectron time-of-flight mass spectrometer (TOF-MS) to be detected with the measurement of the masses and abundances. The details to run the TOF-MS, QMF, and LIT can be found in our previous works.[1-4]

In the ion trap experiments, the cluster ions undergo multiple collisions with the He buffer gas prior to reaction, resulting in efficient thermalization of both their internal and translational energies. The reaction time (t_R) is chosen to be shorter than or comparable to the decay time (τ_R), ensuring that the reactant gas pressure remains nearly constant during the reaction process. Under these conditions, the reaction proceeds from well-defined thermalized ion populations. Variations in reaction time within the experimental time window mainly influence the extent of reaction, while the dominant reaction pathways and product selectivity remain unchanged.

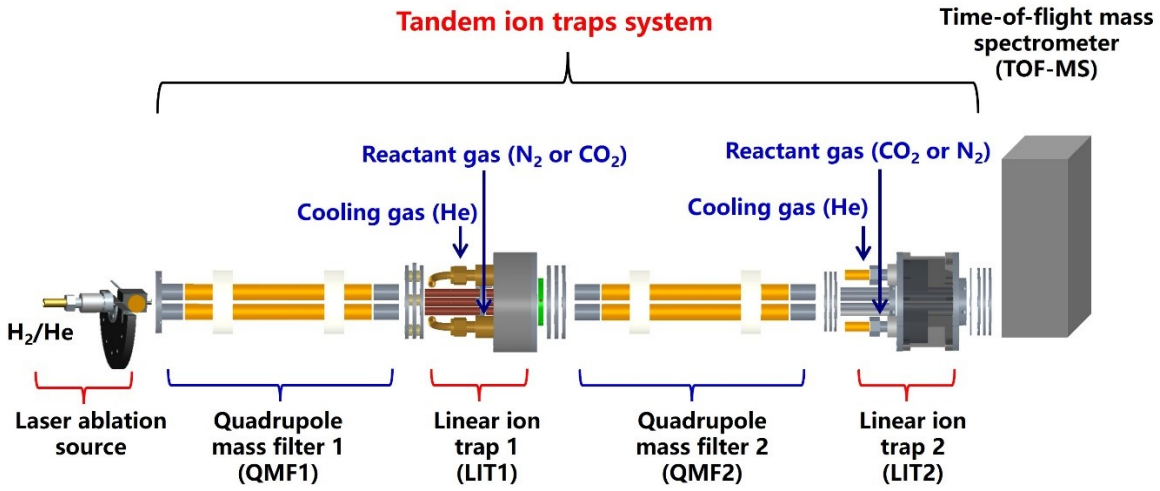

Figure S1. A schematic diagram of the experimental apparatus with a laser-ablation cluster source, a double ion trap system, and a reflectron time-of-flight mass spectrometer.

The collision-induced dissociation (CID) experiments were performed by introducing xenon (Xe) into the LIT2, which was run in the collision-cell mode (rather than the trap mode) for collisions with $Nb_2OH_2N_2CO_2^-$ clusters of which the translation energies could be fixed at different values. Note that $Nb_2OH_2N_2CO_2^-$ clusters were prepared by laser ablation-generated $Nb_2OH_2N_2^-$ reacting with CO_2 in LIT1. The time period for collision of parent clusters with Xe in the LIT2 was short (< 20 μs), and the pressure of Xe in the LIT2 was low (~ 50 mPa). The number of collisions experienced for $Nb_2OH_2N_2CO_2^-$ with Xe was estimated to be 0.1. This means that multiple collisions could be negligible. The daughter and parent ions were detected by the TOF-MS. Note that the daughter ions, such as NC^- and NCO^- from the CID can have very different mass-to-charge ratios (and quite different velocities to enter the TOF-MS) from the parent ions. In this case, the electric potentials on the defection plates in the TOF-MS have to be optimized to get the best signals for the daughter and parent ions separately.

Cryogenic photoelectron imaging spectroscopy. The photoelectron imaging spectroscopy (PEIS) experiments were carried out with a separate TOF-MS equipped with a laser ablation cluster source, a fast flow tube reactor, a cryogenic ion trap, and a photoelectron imaging spectrometer. The metal hydride cluster anions were generated according to the procedure described in the reactivity experiment. After reacting with N_2 in the ion trap reactor for about 10 ms at room temperature, the reactant and product anions were extracted from the trap into the TOF-MS. After mass selection by a mass gate, the cluster anions ($Nb_2OH_4^-$ or $Nb_2OH_2N_4^-$) were photo-detached with a wavelength-tunable laser beam (pulse

width of ~5 ns) delivered from an OPO (optical parametric oscillator) laser source. The kinetic energies (or velocities) of the photo-detached electrons were measured by the photoelectron imaging spectrometer. The details to perform the experiment can be found in a previous study.[5]

1.2 Theoretical Methods.

Density functional theory (DFT) calculations using the Gaussian 16 program package[7] were carried out to investigate the structures of reactant and product ions as well as the reaction mechanisms of corresponding reaction systems $Nb_2OH_4^-/N_2$, $Nb_2OH_2N_2^-/CO_2$, and $Nb_2ON_2^-/CO_2$. The TPSS functional[8] was adopted in this work. The polarized split-valence basis set (6-311+G*)[9-10] for C, N, O, and H atoms and a polarized triple-zeta basis set[11] for valence electrons with an effective core potential[12] for inner shell electrons (Def2-TZVP) for Nb atoms were adopted. The reaction mechanism calculations by the DFT method involved geometry optimization of reaction intermediates and transition states. The relaxed potential energy surface scan was used extensively to obtain good guess structures for intermediates and transition states along the pathways. Vibrational frequency calculations were performed to check that intermediates (IMs) and transition states (TSs) have zero and only one imaginary frequency, respectively. The intrinsic reaction coordinate (IRC) calculations were carried out so that each transition state actually connects two appropriate local minima.[13-14] Natural bond orbital (NBO) analysis was performed with NBO 5.9[15] and the program Multiwfn[16] was employed to analyze orbital compositions by natural atomic orbital methods. The zero-point corrected energies (ΔH_0, enthalpies at 0 K) in unit of eV are reported under the DFT level.

For selected potential energy profiles, the single point energy calculations at the DFT optimized structures were performed by the high-level partially spin-adapted open-shell coupled-cluster method with single, double, and perturbative triple excitations CCSD(T)[17-20] using the Molpro program package.[21] In these CCSD(T) calculations, all the valence electrons were correlated. The reference orbitals for the CCSD(T) calculations were based on the corresponding TPSS Kohn-Sham (KS) orbital rather than the usual Hartree-Fock (HF) orbital because (a) KS orbital has included the electron correlation effect while the HF orbital does not, and (b) using DFT method can avoid the convergence problem of the HF method for transition metals.[22-24] Two augmented double-ζ and triple-ζ correlation consistent basis sets, aug-cc-pVDZ and aug-cc-

pVTZ (denoted as ADZ and ATZ),[25-27] were used for all atoms, and the two-point complete basis set (CBS) limit extrapolations for the total correlation energy were obtained by ADZ-ATZ pair of basis sets based on equation 1,[28] which has been recently found to be superior to alternative extrapolation schemes.[29]

$$E_{total,n} = E_{total,CBS} + \frac{A}{(n+1/2)^4} \quad (1)$$

For the species along the reaction pathway, the electronic energies were from the coupled-cluster method and the zero-point energy (ZPE) corrections were from the frequency calculations by the DFT method. The ZPE corrected energies (ΔH_0, enthalpies at 0 K) in unit of eV are reported in this work.

2. Additional Experimental Results

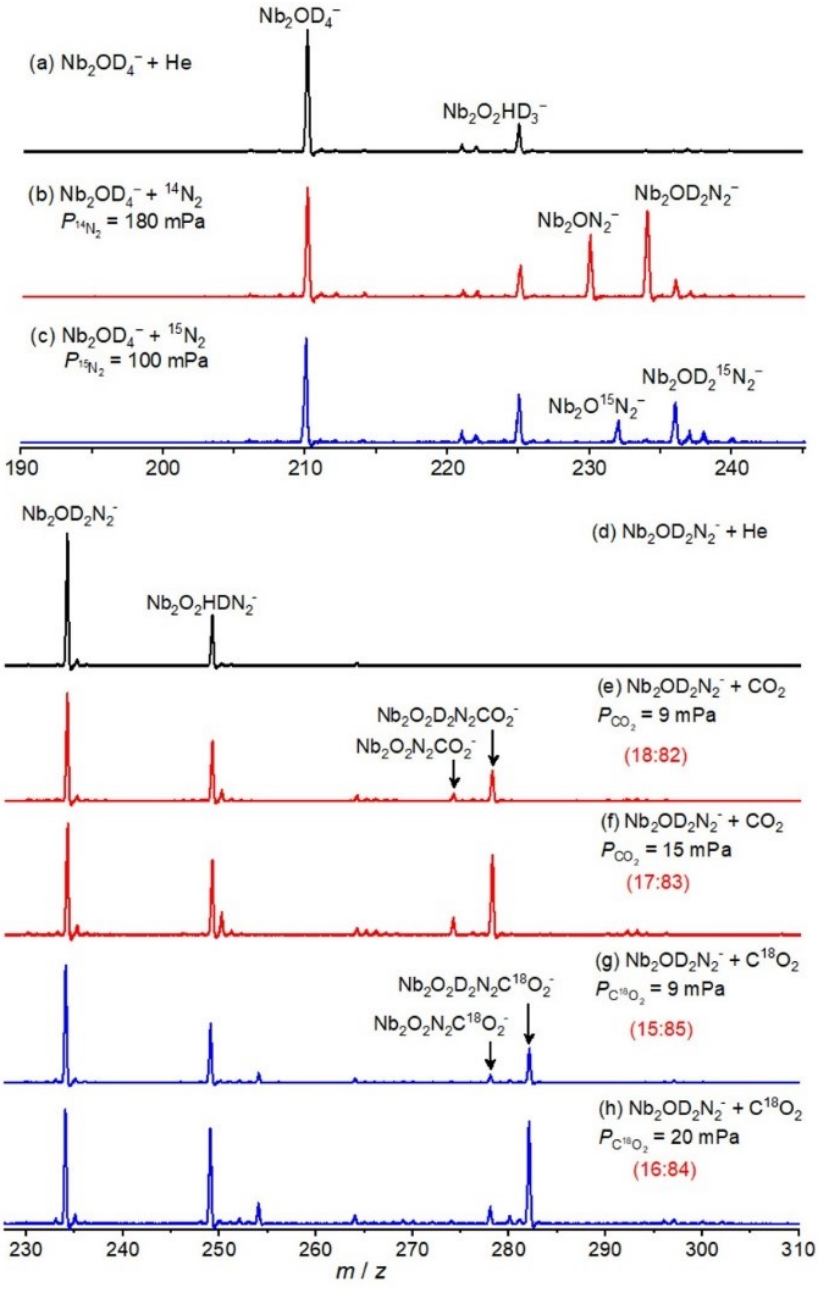

Figure S2. Mass spectra for the reactions of mass-selected $Nb_2OD_4^-$ cluster with He (a), $^{14}N_2$ (b), and $^{15}N_2$ (c), as well as mass selected $Nb_2OD_2N_2^-$ cluster with He (d), $C^{16}O_2$ (e and f), and $C^{18}O_2$ (g and h) at 298 K. The reactant gas pressures are shown. The reaction time is about 1.8 ms. The branching ratios of $Nb_2ON_2CO_2^-$ and $Nb_2OD_2N_2CO_2^-$ are given in parentheses.

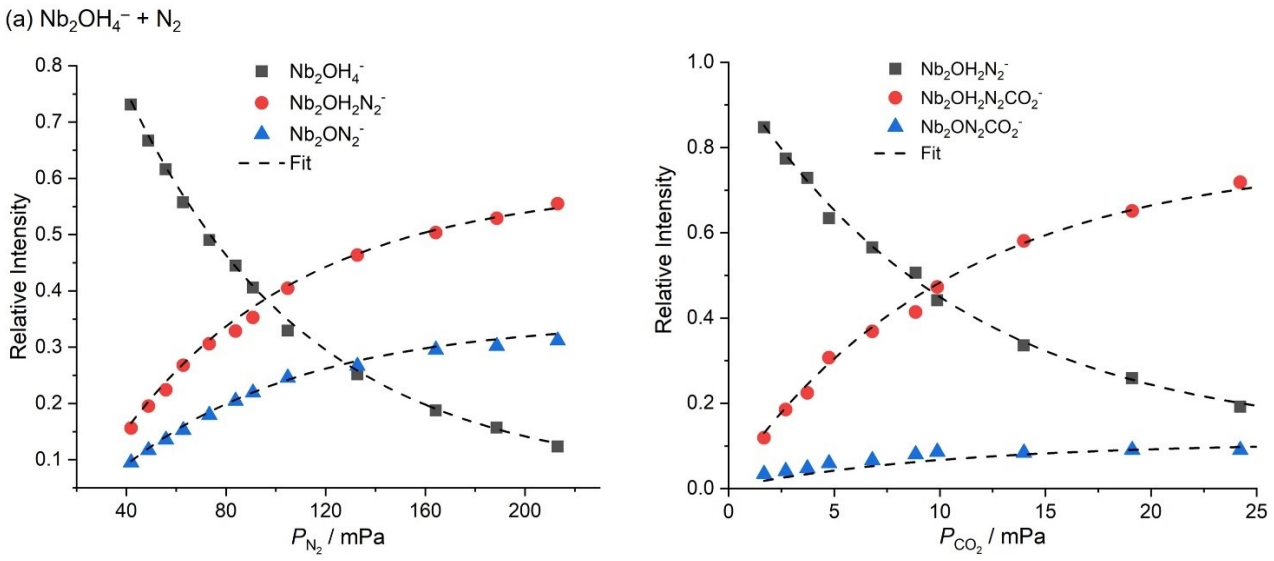

Figure S3. The signal variation of the reactant and product ions with respect to the reactant gas pressures for the reaction systems of $Nb_2OH_4^-/N_2$ (a) and $Nb_2OH_2N_2^-/CO_2$ (b). The reaction time is around 1.8 ms for both systems. The dash lines are fitted to the experimental data points by using the equations derived with the approximation of the pseudo-first-order reaction mechanism for the reactive species.

The pseudo-first-order rate constants (k_1) of the reactions for $Nb_2OH_4^-/N_2$ and $Nb_2OH_2N_2^-/CO_2$ was determined by equation (2), in which I_R is the intensity of the reactant cluster ions after the reaction, I_T is the total ion intensity including product ion contribution, P is the effective pressure of the reactant gas, k_B is the Boltzmann constant, T is the temperature (298 ± 3 K) of the reactant gas, and t_R is the reaction time.

$$\ln\frac{I_R}{I_T} = -k_1\frac{P}{k_B T}t_R \qquad (2)$$

The systematic deviations of t_R (±3%), T (±2%) and P (±20%) were considered to estimate the uncertainty of the k_1 parameter.

The pressure of the reactant gases (CO_2 or N_2, mPa range) is orders of magnitude lower than that of the He buffer gas (Pa range), so the internal energy distribution of the ions is dominated by buffer-gas cooling rather than by the reactant gas. As a result, variations in reactant pressure mainly affect the overall extent of reaction (i.e., product yield), while the observed product distributions and selectivity are governed by intrinsic reaction kinetics and potential energy surfaces.

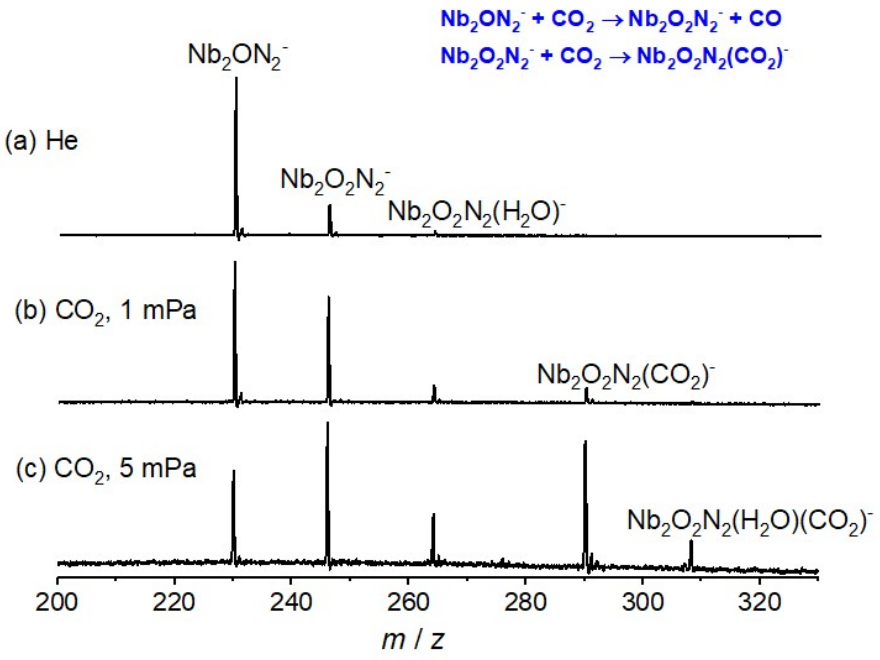

Figure S4. Mass spectra for the reactions of mass-selected $Nb_2ON_2^-$ cluster with He (a), 1 mPa CO_2 (b), and 5 mPa CO_2 (c). The reaction time is about 1.8 ms.

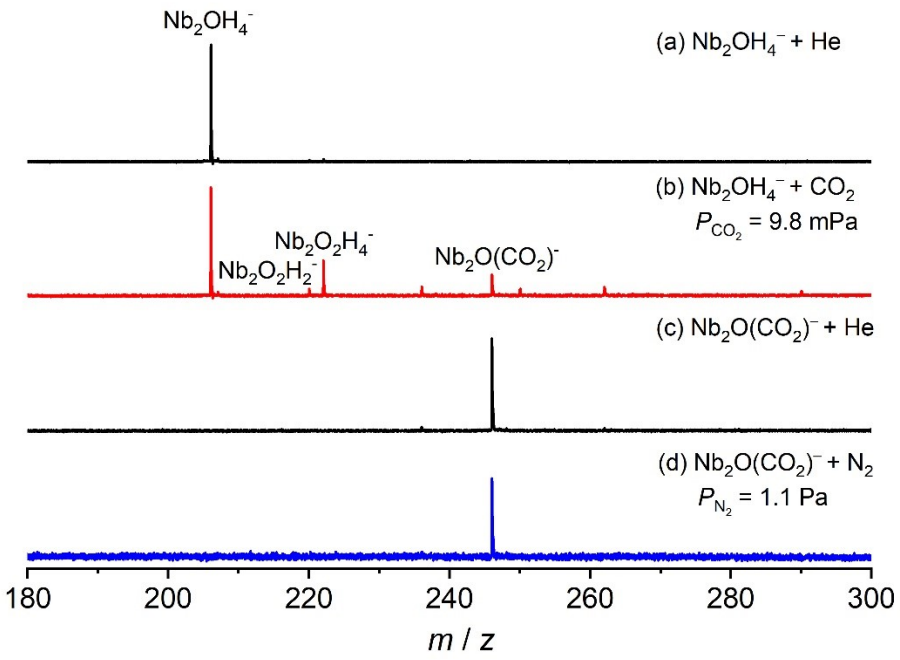

Figure S5. Mass spectra for the reactions of mass-selected $Nb_2OH_4^-$ cluster with He (a) and CO_2 (b), as well as the mass-selected $Nb_2O(CO_2)^-$ cluster with He (c) and N_2 (d) at 298 K. The reaction times are 2 ms for (b) and 13 ms for (d). The reactant gas pressures are shown.

3. Additional Theoretical Results

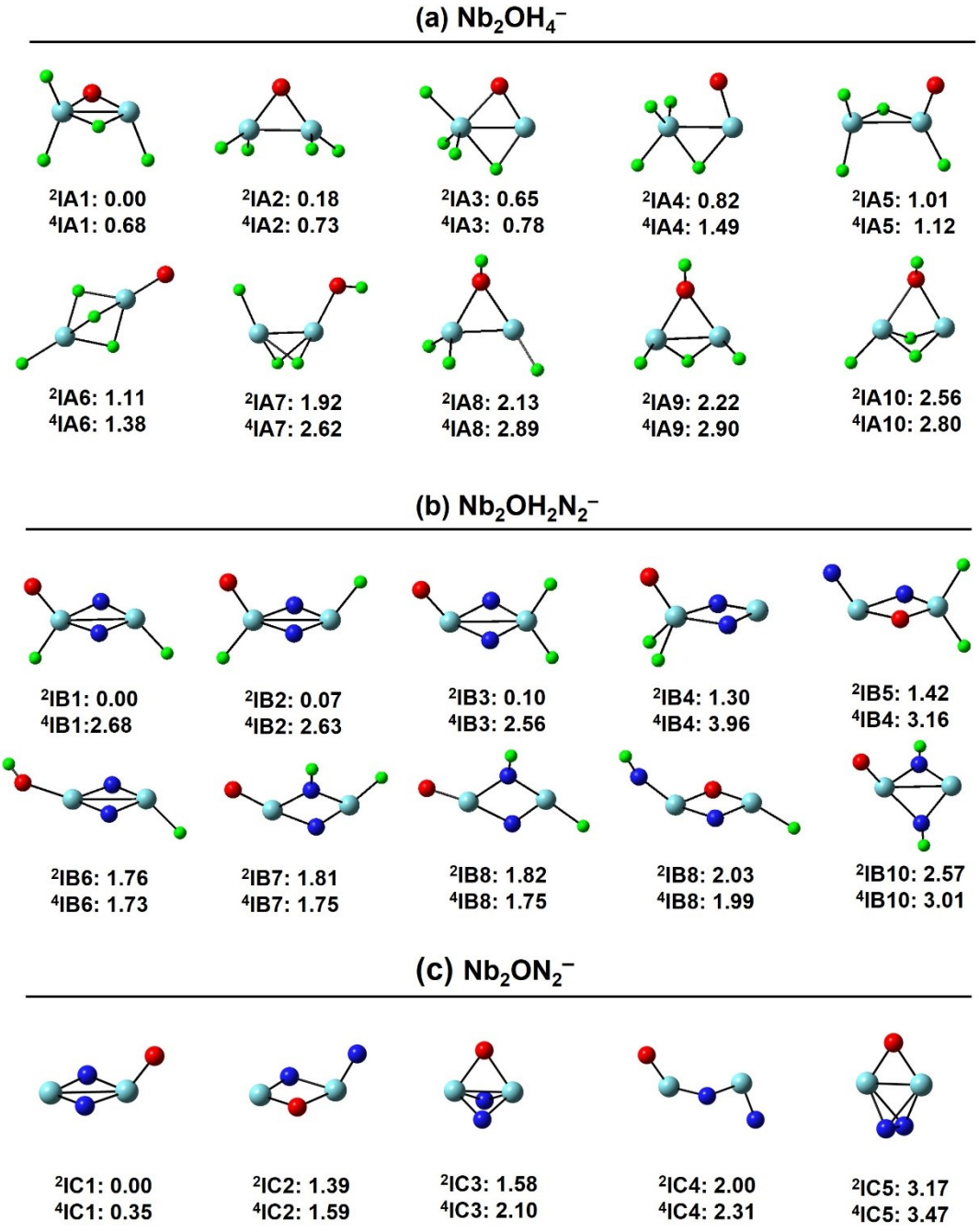

Figure S6. Isomeric structures of $Nb_2OH_4^-$ (a), $Nb_2OH_2N_2^-$ (b), and $Nb_2ON_2^-$ (c) optimized by DFT at TPSS level. The zero-point vibration corrected relative energies (ΔH_0, eV) at the RCCSD(T)/CBS level are given. The superscripts represent spin multiplicities.

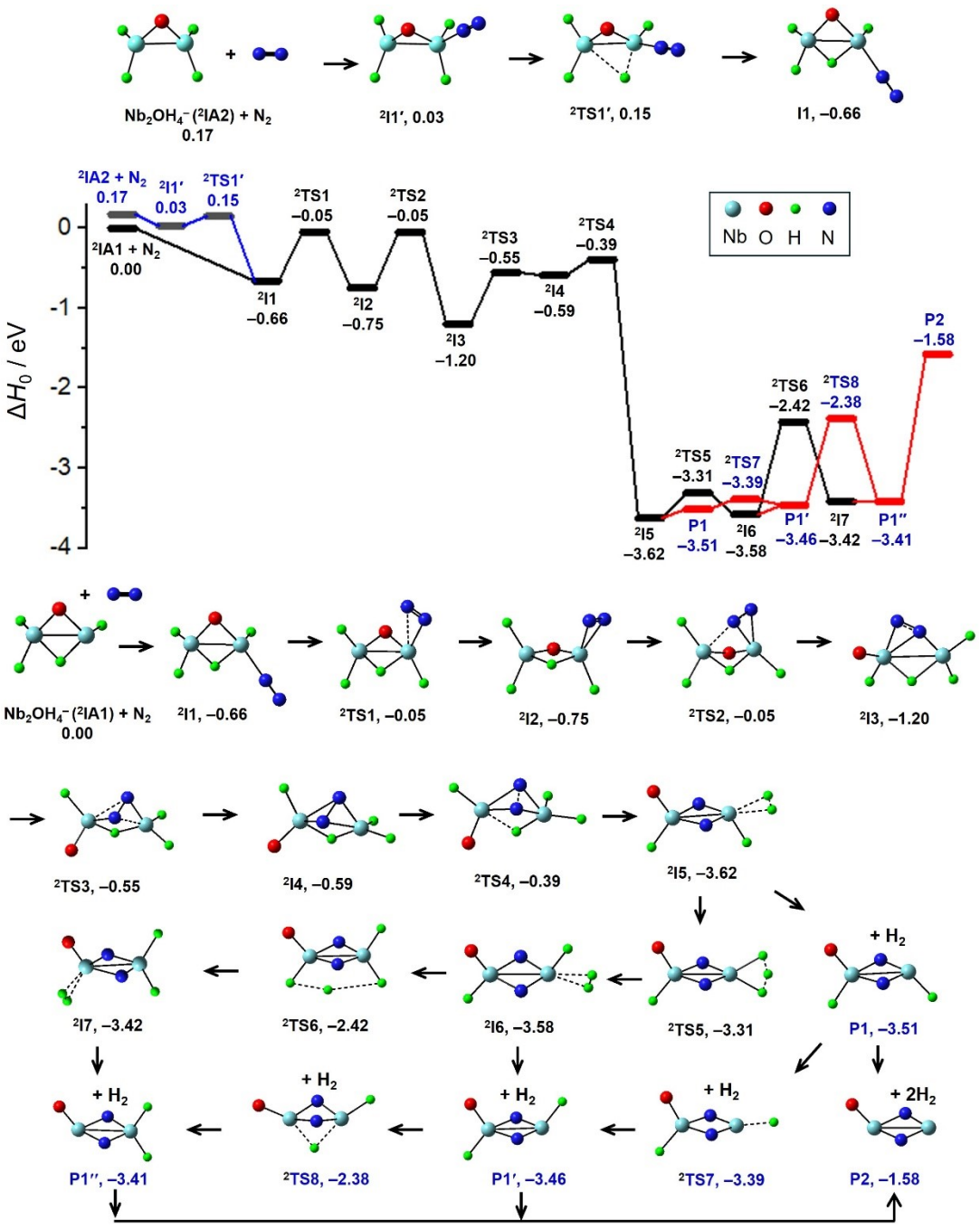

Figure S7. The most favorable potential energy profile for the reaction of $Nb_2OH_4^-$ with N_2 calculated by DFT at TPSS level. The relative energies (ΔH_0, eV) with respect to the separated reactants are given at the RCCSD(T)/CBS level. The structures of reaction intermediates, transition states, and products are shown. The superscripts represent spin multiplicities.

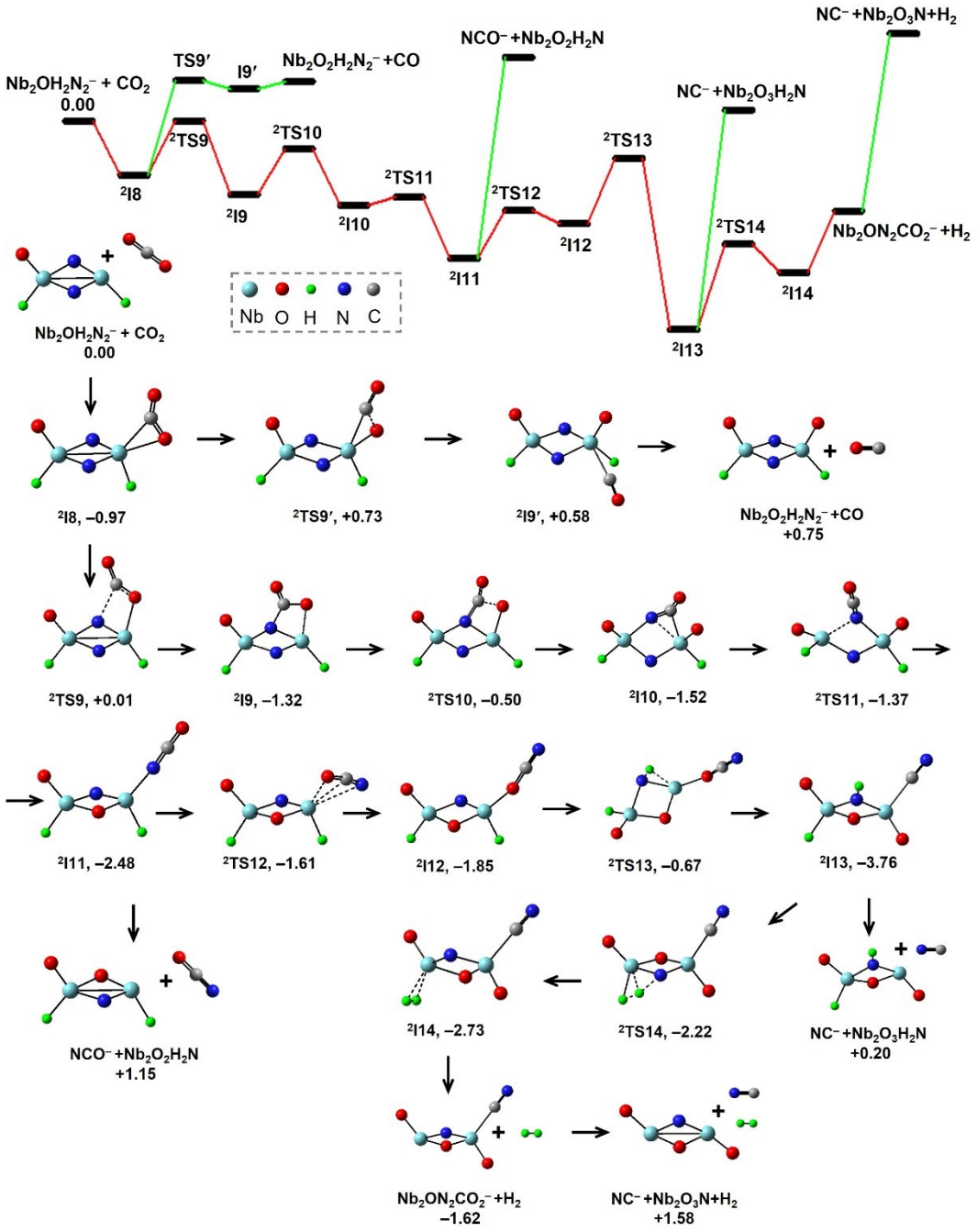

Figure S8. The potential energy profiles for the reaction of $Nb_2OH_2N_2^-$ with CO_2 calculated by DFT at TPSS level. The relative energies (ΔH_0, eV) with respect to the separated reactants are given at the RCCSD(T)/CBS level. The structures of reaction intermediates, transition states, and products are shown. The superscripts represent spin multiplicities.

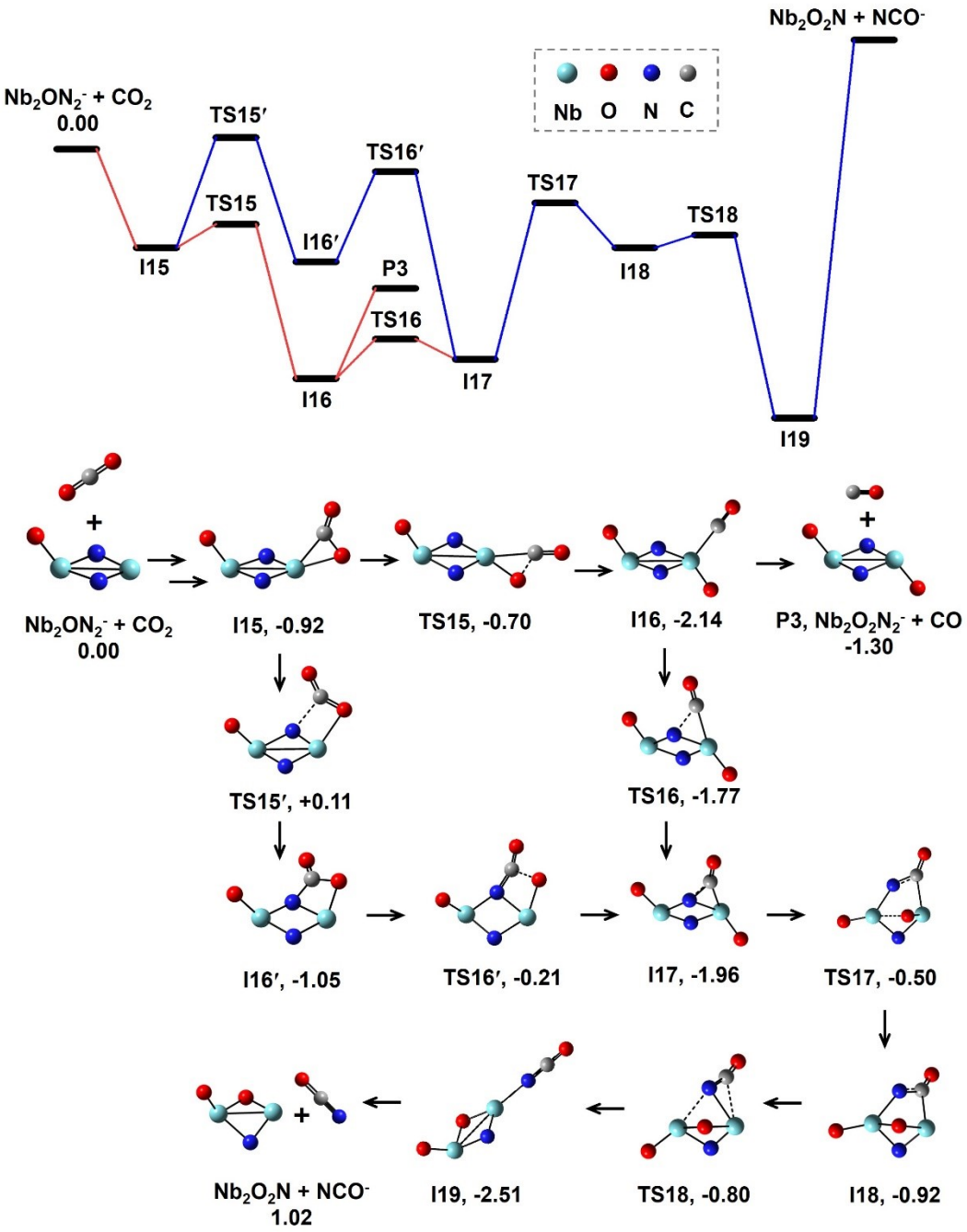

Figure S9. The potential energy profile for the reaction of $Nb_2ON_2^-$ with CO_2 calculated by DFT at TPSS level. The relative energies (ΔH_0, eV) with respect to the separated reactants are given at the RCCSD(T)/CBS level. The structures of reaction intermediates, transition states, and products are shown. The superscripts represent spin multiplicities.

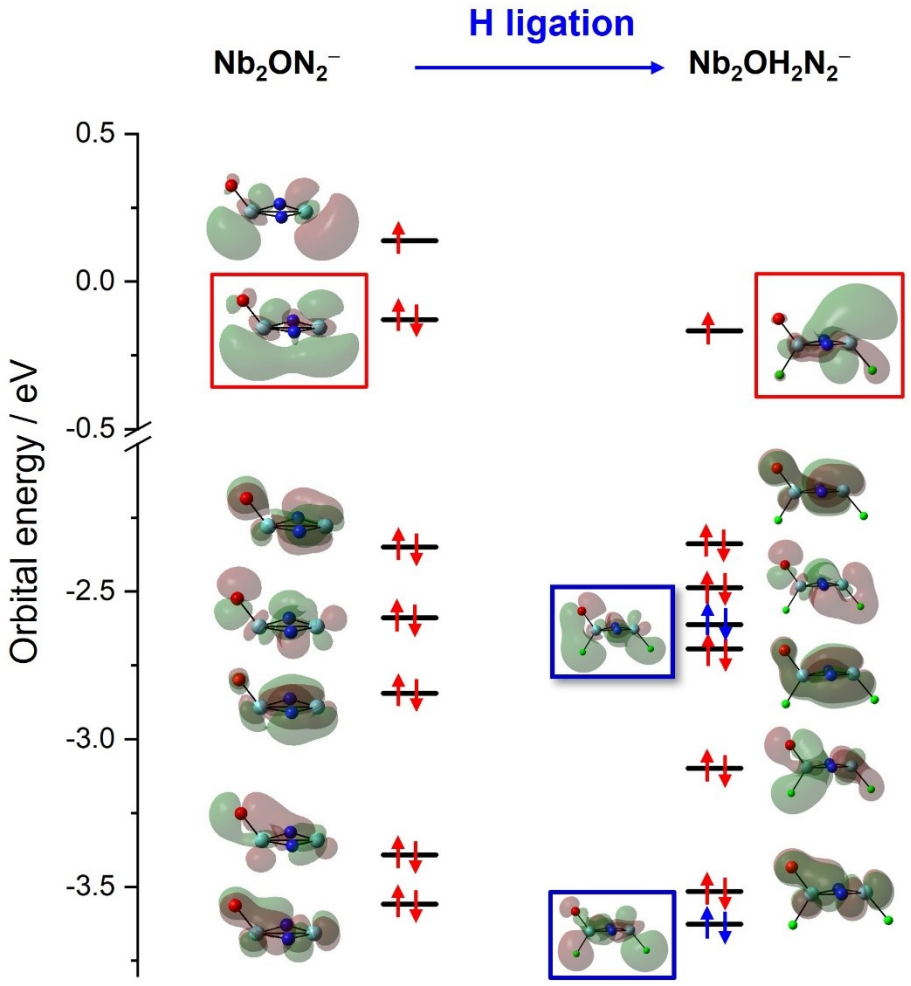

Figure S10. Molecular orbital (MO) analysis for $Nb_2ON_2^-$ and $Nb_2OH_2N_2^-$. The MOs marked with a blue border denote the newly formed orbitals upon the ligation of H atoms. The MOs marked with a red border denote the active orbitals that interact strongly with CO_2 in the reactions.

Table S1. Relative energies of key intermediates and transition states for C–N coupling and O–CO cleavage in the $Nb_2OH_2N_2^-/CO_2$ and $Nb_2ON_2^-/CO_2$ systems using different DFT functionals. The high-level CCSD(T)/CBS energies are given in brackets.

	Relative energies/eV		
	TPSS	B3LYP	PBE0
$Nb_2OH_2N_2^- + CO_2$	0.00	0.00	0.00
I8	–1.04 [–0.97]	–0.83 [–0.95]	–0.89 [–0.94]
TS9	–0.16 [0.01]	0.11 [0.01]	0.12 [0.00]
I9	–1.23 [–1.32]	–1.18 [–1.29]	–1.46 [–1.29]
TS9′	0.23 [0.73]	0.66 [0.52]	0.89 [0.05]
I9′	–0.38 [0.58]	–0.04 [0.05]	0.26 [–0.15]
$Nb_2ON_2^- + CO_2$	0.00	0.00	0.00
I15	–2.03 [–0.92]	–1.40 [–0.90]	–1.82 [–0.98]
TS15	–1.94 [–0.70]	–1.24 [–0.68]	–1.53 [–0.61]
I16	–2.57 [–2.14]	–1.87 [–2.13]	–2.06 [–2.13]
TS15′	–0.09 [0.11]	0.07 [–0.12]	0.07 [0.12]
I16′	–1.15 [–1.05]	–0.90 [–0.68]	–0.90 [–0.91]

Table S2. Wiberg bond order analysis for the C−N coupling process in the reaction systems of $Nb_2OH_2N_2^-/CO_2$ and $Nb_2ON_2^-/CO_2$.

Wiberg bond order	**$Nb_2OH_2N_2^- + CO_2$**	**$Nb_2ON_2^- + CO_2$**
	^{2}I8 → ^{2}TS9 → **^{2}I9**	**^{2}I15** → ^{2}TS15′ → **^{2}I16′**
Nb1−C	**0.4** → 0.1 → **0.0**	**0.8** → 0.2 → **0.0**
C−N1	**0.0** → 0.2 → **1.0**	**0.0** → 0.3 → **1.1**
Nb1−N1	**1.8** → 1.5 → **0.7**	**1.8** → 1.6 → **0.7**
$C-O_{(CO2)}$	**1.4** → 1.3 → **1.1**	**1.1** → 1.5 → **1.1**

4. References

1. Wu, X.-N.; Xu, B.; Meng, J.-H.; He, S.-G., C–H Bond Activation by Nanosized Scandium Oxide Clusters in Gas-Phase. *Int. J. Mass Spectrom.* **2012**, *310*, 57-64.

2. Yuan, Z.; Zhao, Y.-X.; Li, X.-N.; He, S.-G., Reactions of $V_4O_{10}^+$ Cluster Ions with Simple Inorganic and Organic Molecules. *Int. J. Mass Spectrom.* **2013**, *354*, 105-112.

3. Yuan, Z.; Li, Z.-Y.; Zhou, Z.-X.; Liu, Q.-Y.; Zhao, Y.-X.; He, S.-G., Thermal Reactions of $(V_2O_5)_NO^-$ (N = 1–3) Cluster Anions with Ethylene and Propylene: Oxygen Atom Transfer Versus Molecular Association. *J. Phys. Chem. C* **2014**, *118*, 14967-14976.

4. Jiang, L. X.; Liu, Q. Y.; Li, X. N.; He, S. G. Design and Application of a High-Temperature Linear Ion Trap Reactor. *J. Am. Soc. Mass Spectrom.* **2018**, *29*, 78-84.

5. Liu, Q.-Y.; Hu, L.; Li, Z.-Y.; Ning, C.-G.; Ma, J.-B.; Chen, H.; He, S.-G., Photoelectron Imaging Spectroscopy of MoC^- and NbN^- Diatomic Anions: A Comparative Study. *J. Chem. Phys.* **2015**, *142*.

6. Kim, J. B.; Weichman, M. L.; Neumark, D. M. Structural Isomers of Ti_2O_4 and Zr_2O_4 Anions Identified by Slow Photoelectron Velocity-Map Imaging Spectroscopy. *J. Am. Chem. Soc.* **2014**, *136*, 7159-7168.

7. Frisch, M. J. T., G. W.; Schlegel, H. B.; Scuseria, G. E.; Robb, M. A.; Cheeseman, J. R.; Scalmani, G.; Barone, V.; Mennucci, B.; Petersson, G. A.; Nakatsuji, H.; Caricato, M.; Li, X.; Hratchian, H. P.; Izmaylov, A. F.; Bloino, J.; Zheng, G.; Sonnenberg, J. L.; Hada, M.; Ehara, M.; Toyota, K.; Fukuda, R.; Hasegawa, J.; Ishida, M.; Nakajima, T.; Honda, Y.; Kitao, O.; Nakai, H.; Vreven, T.; Montgomery, J. A., Jr.; Peralta, J. E.; Ogliaro, F.; Bearpark, M.; Heyd, J. J.; Brothers, E.; Kudin, K. N.; Staroverov, V. N.; Kobayashi, R.; Normand, J.; Raghavachari, K.; Rendell, A.; Burant, J. C.; Iyengar, S. S.; Tomasi, J.; Cossi, M.; Rega, N.; Millam, J. M.; Klene, M.; Knox, J. E.; Cross, J. B.; Bakken, V.; Adamo, C.; Jaramillo, J.; Gomperts, R.; Stratmann, R. E.; Yazyev, O.; Austin, A. J.; Cammi, R.; Pomelli, C.; Ochterski, J. W.; Martin, R. L.; Morokuma, K.; Zakrzewski, V. G.; Voth, G. A.; Salvador, P.; Dannenberg, J. J.; Dapprich, S.; Daniels, A. D.; Farkas, O.; Foresman, J. B.; Ortiz, J. V.; Cioslowski, J.; Fox, D. J., Gaussian 09, Revision A.1, Gaussian, Inc., Wallingford Ct, 2009., G09.

8. Perdew, J. P.; Wang, Y., Accurate and Simple Analytic Representation of the Electron-Gas Correlation Energy. *Phys. Rev. B* **1992**, *45*, 13244-13249.

9. Hehre, W. J.; Ditchfield, R.; Pople, J. A., Self-Consistent Molecular Orbital Methods. Xii. Further Extensions of Gaussian-Type Basis Sets for Use in Molecular Orbital Studies of Organic Molecules. *J. Chem. Phys.* **1972**, *56*, 2257-2261.

10. Krishnan, R.; Binkley, J. S.; Seeger, R.; Pople, J. A., Self-Consistent Molecular Orbital Methods. Xx. A Basis Set for Correlated Wave Functions. *J. Chem. Phys.* **1980**, *72*, 650-654.

11. Weigend, F.; Ahlrichs, R., Balanced Basis Sets of Split Valence, Triple Zeta Valence and Quadruple Zeta Valence Quality for H to Rn: Design and Assessment of Accuracy. *Phys. Chem. Chem. Phys.* **2005**, *7*, 3297-3305.

12. Andrae, D.; Häußermann, U.; Dolg, M.; Stoll, H.; Preuß, H., Energy-Adjusted Ab Initio Pseudopotentials for the 2nd and 3rd Row Transition-Elements. *Theor. Chim. Acta* **1990**, *77*, 123-141.

13. Gonzalez, C.; Schlegel, H. B., An Improved Algorithm for Reaction-Path Following. *J. Chem. Phys.* **1989**, *90*, 2154-2161.

14. Gonzalez, C.; Schlegel, H. B., Reaction Path Following in Mass-Weithted Internal Coordinates. *J. Phys. Chem.* **1990**, *94*, 5523-5527.

15. Glendening, E. D.; Badenhoop, J. K.; Reed, A. E.; Carpenter, J. E.; Bohmann, J. A.; Morales, C. M.; Weinhold, F., Theoretical Chemistry Institute, University of Wisconsin: Madison, Wi; Http://Www.Chem.Wisc.Edu/, 2012.

16. Lu, T.; Chen, F., Multiwfn: A Multifunctional Wavefunction Analyzer. *J. Comput. Chem.* **2012**, *33*, 580-592.

17. III, G. D. P.; Bartlett, R. J., A Full Coupled‐Cluster Singles and Doubles Model: The Inclusion of Disconnected Triples. *J. Chem. Phys.* **1982**, *76*, 1910-1918.

18. Raghavachari, K.; Trucks, G. W.; Pople, J. A.; Head-Gordon, M., A Fifth-Order Perturbation Comparison of Electron Correlation Theories. *Chem. Phys. Lett.* **1989**, *157*, 479-483.

19. Watts, J. D.; Gauss, J.; Bartlett, R. J., Coupled‐Cluster Methods with Noniterative Triple Excitations for Restricted Open‐Shell Hartree–Fock and Other General Single Determinant Reference Functions. Energies and Analytical Gradients. *J. Chem. Phys.* **1993**, *98*, 8718-8733.

20. Knowles, P. J.; Hampel, C.; Werner, H. J., Coupled Cluster Theory for High Spin, Open Shell Reference Wave Functions. *J. Chem. Phys.* **1993**, *99*, 5219-5227.

21. Werner, H.-J. K., P. J.; Lindh, R.; Manby, F. R.; Schutz, M.; Celani, P.; Korona, T.;; Mitrushenkov, A. R., G.; Adler, T. B.; Amos, R. D.; Bernhardsson, A.; Berning, A.; Cooper, D.; L.; Deegan, M. J. O. D., A. J.; Eckert, F.; Goll, E.; Hampel, C.; Hetzer, G.; Hrenar, T.; Knizia,; G.; Koppl, C. L., Y.; Lloyd, A. W.; Mata, R. A.; May, A. J.; McNicholas, S. J.; Meyer, W.; Mura,; M. E.; Nicklass, A. P., P.; Pfluger, K.; Pitzer, R.; Reiher, M.; Schumann, U.; Stoll, H.; Stone,; A. J.; Tarroni, R. T., T.; Wang, M.; Wolf, A. , Molpro, Version 2010.1, a Package of Ab Initio Programs. See Http://Www.Molpro.Net.

22. Sun, Y.; Tang, H.; Chen, K.; Hu, L.; Yao, J.; Shaik, S.; Chen, H., Two-State Reactivity in Low-Valent Iron-Mediated C–H Activation and the Implications for Other First-Row Transition Metals. *J. Am. Chem. Soc.* **2016**, *138*, 3715-3730.

23. Carreón-Macedo, J.-L.; Harvey, J. N., Computational Study of the Energetics of $^{3}fe(Co)_4$, $^{1}fe(Co)_4$ and $^{1}fe(Co)_4(L)$, L = Xe, Ch_4, H_2 and Co. *Phys. Chem. Chem. Phys.* **2006**, *8*, 93-100.

24. Villaume, S.; Daniel, C.; Strich, A.; Perera, S. A.; Bartlett, R. J., Quantum Chemical Study of the Electronic Structure of $Nich_2^+$ in Its Ground State and Low-Lying Electronic Excited States. *J. Chem. Phys.* **2005**, *122*, 044313.

25. Kendall, R. A.; Jr., T. H. D.; Harrison, R. J., Electron Affinities of the First‐Row Atoms Revisited. Systematic Basis Sets and Wave Functions. *J. Chem. Phys.* **1992**, *96*, 6796-6806.

26. Jr., T. H. D., Gaussian Basis Sets for Use in Correlated Molecular Calculations. I. The Atoms Boron through Neon and Hydrogen. *J. Chem. Phys.* **1989**, *90*, 1007-1023.

27. Balabanov, N. B.; Peterson, K. A., Systematically Convergent Basis Sets for Transition Metals. I. All-Electron Correlation Consistent Basis Sets for the 3d Elements Sc–Zn. *J. Chem. Phys.* **2005**, *123*, 064107.

28. Martin, J. M. L., Ab Initio Total Atomization Energies of Small Molecules — Towards the Basis Set Limit. *Chem. Phys. Lett.* **1996**, *259*, 669-678.

29. Feller, D.; Peterson, K. A.; Hill, J. G., On the Effectiveness of Ccsd(T) Complete Basis Set Extrapolations for Atomization Energies. *J. Chem. Phys.* **2011**, *135*, 044102.